??卷?期 结 构 化 学（*JIEGOU HUAXUE*）(投稿模板) Vol. ??, No.?
????.? *Chinese J. Struct. Chem.* ???~???

Role of Microstructure and Spectrum Features on the Catalysis Effect of $Ce_{1-x}(Nd_{0.5}Eu_{0.5})_xO_{2-\delta}$ Solid Solutions

ZHANG Guo-Fang (张国芳);HOU Zhong-Hui(侯忠辉);ZHAI Ting-Ting(翟亭亭);XV Jian-Yi(许剑轶);ZHANG Yang-Huan(张羊换)

School of Material and Metallurgy, Inner Mongolia University of Science and Technology, Baotou 014010, *China*

ABSTRACT Nanosized $Ce_{1-x}(Nd_{0.5}Eu_{0.5})_xO_{2-\delta}$ solid solutions (x = 0.00～0.20) were synthesized by means of hydrothermal method. Then the solid solutions were ball milled with Mg_2Ni and Ni powders for 20 h to get the Mg_2Ni–Ni–5 mol% $Ce_{1-x}(Nd_{0.5}Eu_{0.5})_xO_{2-\delta}$ composites. The structures and spectrum characteristics of the $Ce_{1-x}(Nd_{0.5}Eu_{0.5})_xO_{2-\delta}$ solid solutions catalysts were analyzed systemically. XRD results showed that the doped samples exhibited single phase of CeO_2 fluorite structure. The cell parameters and cell volumes were increased with increasing the doped content. Raman spectrum revealed that the peak position of F_{2g} mode shift to higher wavenumbers and the peak corresponding to oxygen vacancies were observed distinctly for the doped samples. UV-Vis technique indicated that the absorption peaks of Eu^{3+} and Nd^{3+} ions appeared; the bandgap energy was decreased linearly. The electrochemical and kinetic properties of the Mg_2Ni–Ni–5 mol% $Ce_{1-x}(Nd_{0.5}Eu_{0.5})_xO_{2-\delta}$ composites were measured. The maximum discharge capacity was increased from 722.3 mAh/g for x = 0.00 to 819.7 mAh/g for x = 0.16, and the cycle stability S_{20} increased from 25.0% (x = 0.00) to 42.2% (x = 0.20). The kinetic measurement proved that the catalytic activity of composite surfaces and the hydrogen diffusion rate were improved for the composites with doped catalysts, especially for the composites with x = 0.16 and x = 0.20. The catalysis mechanism was analyzed from the point of microstructure and spectrum features of the $Ce_{1-x}(Nd_{0.5}Eu_{0.5})_xO_{2-\delta}$ solid solutions.

Keywords: hydrothermal method; $Ce_{1-x}(Nd_{0.5}Eu_{0.5})_xO_{2-\delta}$ solid solutions; Mg_2Ni; ball milling; catalysis mechanism; DOI: 10.14102/j.cnki.0254-5861.2011-1694

1 INTRODUCTION

Nowadays, researches on the hydrogen storage properties of Mg-based alloys have attracted much attention due to their high theoretical hydrogen storage capacity, earth abundance and low cost. However, there are still some drawbacks which hindered the practical applications as the negative electrode materials of Ni/MH batteries, such as the poor cycle stabilities and the slow sorption/desorption kinetics. Researchers have devoted numerous efforts to overcome these limitations. Generally, the hydrogen storage properties of Mg-based alloys could be improved by nanocrystallizing the alloys and/or adding various catalysts or additives[1, 2]. Ball milling method is one of the most effective and simple ways to get nanosized materials with more fresh surface areas and a large number of defects on the surface and in the bulk of alloys powders[3]. On the other hand, many kinds of catalysts have been chosen to add into the Mg-based systems and exhibit outstanding catalysis properties. Metal oxides are a kind of the most important and effective catalysts which have been extensively investigated. Compared with the metal catalysts, the metal oxides could disperse uniformly on the surface of the Mg-based alloys due to their brittleness. In addition, the effect of local electronic structure of the catalysts also plays an important role[4, 5]. It was reported that the oxides were reduced to lower valence and the local structures were disarranged after ball milled with MgH_2[6]. The interaction between the metal oxide catalysts and the surface of Mg-based hydride might improve the desorption kinetic properties[7].

Over the past decades, the catalysis properties of CeO_2 and CeO_2 based materials have been researched sufficiently due to their unique structures and special electronic characteristics. Thus, CeO_2 based materials have been widely used in various fields, such as the three-way catalysts (TWC)[8, 9], the water gas shift catalysts (WGS)[10], and the application of many oxidation catalysts[11, 12]. Generally speaking, the catalysis effects rely primarily on the activity of the redox couple Ce^{4+}/Ce^{3+}, which is relatively easier to change the valence of the Ce ions (1.3～1.8 V) under different conditions than other metal oxides. Meanwhile, the other specific feature is the formation of oxygen vacancies ($V_O^{\bullet\bullet}$) in the bulk or on the surface of CeO_2 which can influence the catalysis effect evidently. Additionally, various cations whose ionic radii and valence are different from those of Ce ions were chosen to dope into the lattice of CeO_2 so as to obtain the CeO_2-based solid solutions. Their addition would induce extra oxygen vacancies and the structure distortion, and it was proved that a kind of active phase was formed at the interface of catalyst. These changes usually mean the improvement of the catalysis effects[13-15]. A mountain of researches showed that doping di- or trivalent ions into the lattice of CeO_2 is a primary way to improve their catalysis activities obviously. The doped ions could partially replace Ce^{4+} and generate a large amount of oxygen vacancies in the lattice[16-18].

It has been reported that CeO_2 has the ability to react with H_2[11]. The application of CeO_2-based catalysts in the hydrogen storage field has also attracted much more attention. But the opinions are various on the catalysis mechanism. There were several reports about the catalysis effect of CeO_2 on the hydrogen storage properties of Mg-based alloy. Researchers have found the effective impact of CeO_2 on MgH_2 sorption properties[19]. And it is noteworthy that the pure CeO_2 seems to have no effect on the hydrogen desorption

kinetic, but a positive effect was observed for Pt doped CeO_2[20]. Jelena et al.[21] studied the influence of nanosized CeO_2 on the hydrogen desorption properties of MgH_2. They attributed the catalysis effect to the nonstoichiometric and the vacant structure of CeO_2, which means that the oxygen vacancies existed in the lattice of CeO_2 and the small polarons could act as the promoter to increase the catalytic activity. From the microcosmic point of view, the H atom usually tends to penetrate along the (110) face of CeO_2[22], then a kind of electronic exchange reaction occurred between the Mg-based hydride and the catalysts which could decrease the bond energy of Mg–H. As a consequence, the kinetic of hydrogen desorption reaction was improved. Our group had investigated the catalysis effects of doped and un-doped CeO_2 on the hydrogen storage properties of Mg-based alloy. It was found that doped CeO_2 solid solutions always do well on it. Their catalysis performances were linked closely with the species of the doped ions and the doped content. Beyond that, the spectra and structure characteristics of the catalysts also play an important role during the catalysis process [23]. But the roles of impact factors such as the crystal structure, the spectral characteristics and the electronic structure during the catalysis reactions are still unclear.

It has been reported that the Nd^{3+}-doped CeO_2 has the highest hole conductivity[24], and the formed solid solutions show higher catalytic activity for the total oxidation of methane[25]. On the other hand, it was also reported that $Ce_{1-x}Eu_xO_{2-x/2}$ mixed oxides have better catalytic performances for the oxidation of CO, which was attributed to the increased amount of oxygen vacancies[26]. Thus, in this paper, we synthesized Nd^{3+} and Eu^{3+} ions co-doped nanosized CeO_2-based solid solution catalysts. The crystalline structures and spectral features were investigated systematically. The catalysis effects on the electrochemical performance of ball milled Mg_2Ni were evaluated, and the catalysis mechanism was analyzed from the viewpoints of microstructure and spectrum features of the oxide catalysts.

2 EXPERIMENTAL

2. 1 Syntheses of the samples

$Ce(NO_3)_3·6H_2O$ (AR), $Nd(NO_3)_3·6H_2O$ (AR), $Eu(NO_3)_3·6H_2O$ (AR) and NaOH (AR) were used as the starting reagents to synthesize the Nd^{3+} and Eu^{3+} ions co-doped $Ce_{1-x}(Nd_{0.5}Eu_{0.5})_xO_{2-\delta}$ solid solutions via hydrothermal method. The specific hydrothermal synthetic process was described as follows: solutions of the lanthanide nitrate were confected to 0.3 mol/L, respectively. Then these three kinds of solutions were mixed and stirred in certain proportion. The dopant content x varied from 0.00 to 0.20. After that, 6 mol/L NaOH solution was used as the mineralizer to adjust the pH value to around 12. The received suspensions were sealed in the Teflon-lined autoclaves and heated to 200 ℃ for 24 h. The obtained products were washed fully with distilled water and dried at 80 ℃ for 6 h. Afterwards, the as-prepared $Ce_{1-x}(Nd_{0.5}Eu_{0.5})_xO_{2-\delta}$ solid solutions

were mixed with Mg_2Ni powders (200 mesh) and Ni powders (200 mesh) with the weight ration of 0.05:1:1 and ball milled for 20 h. The ball milling process was held in stainless-steel containers in the Ar atmosphere, with the weight ratio of balls to the mixed materials to be 40:1 and the rotating speed of the jars kept at 350 rmp/min.

2. 2 Characterization

The phases of the solid solutions were measured by X-ray diffractometer (Rigaku DAMX2500) with Cu$K\alpha$ radiation. The average particle size D was calculated from the diffraction peak (111) of CeO_2 utilizing the Scherrer formula, and the lattice parameters were estimated by full-matrix least-squares methods. The Diffuse reflectance UV-visible spectroscopy of the samples was recorded on Hitachi U-3900 UV-vis spectrophotometer. Raman spectra of the samples were measured on a JY-HR800 Raman spectrometer with a He-Ne ions laser in the region of 200～1000 cm^{-1}. The excitation wavelength was 418 nm and the output powder was 20 mW. The experimental details of the electrochemistry and the kinetic properties of Mg_2Ni-based compounds were almost the same as described in our precious report[23]. The weight of Mg_2Ni alloys was deemed as the active material.

3 RESULTS AND DISCUSSION

3. 1 XRD characterization

Fig. 1 shows the XRD patterns of pure and Nd^{3+}/ Eu^{3+} co-doped CeO_2 samples. All the samples with the doped content x ranging from 0.00 to 0.20 exhibited typical fluorite cubic structure with space group $fm3m$ and no phases corresponding to the compounds of the doped ions were observed. Although the structures of the solid solutions keep the single phase, the doped ions still induce the subtle transformation of the lattice structure. Inset of Fig. 1 shows the enlarged patterns of the (111) peak. Compared with the undoped CeO_2, the diffraction pattern of this peak gradually shifts towards the lower angle range, implying the lattice expansion follows the Vegard's law. It should also be noted that the (111) peak of the sample with x = 0.20 slightly shifts to the higher angle, which could be attributed to the crystalline size effect (Fig. 2(c)). The lattice parameters are one of the most sensitive indexes to reflex the changes of the lattice structure and the chemical composition. Meanwhile, it is usually used to estimate the solid solubility[27]. We all know that both of the doped ionic radii of Eu^{3+} (1.066 Å) and Nd^{3+} (1.109 Å) are larger than that of Ce^{4+} (0.97 Å) in 8-coordination. If the doped ions incorporate into the lattice and replace the site of Ce^{4+}, the cell parameters and the cell volumes will increase. Indeed, a systemic increase of cell parameters with the doped content can certainly be discernible from Fig. 2(a), and similar tendency is also observed for the cell volumes, as shown in Fig. 2(b). These results confirm that the doped ions have incorporated into the lattice of CeO_2 and the homogenous $Ce_{1-x}(Nd_{0.5}Eu_{0.5})_xO_{2-\delta}$ solid solutions are formed. Fig. 2(c) exhibits the crystalline size of the solid solutions calculated from the Scherrer

formula. The size is largely influenced by the doped content. Firstly, the size decreased abruptly from 23 nm for pure CeO_2 to 12 nm for the sample with doped content x = 0.04. Further increasing the doped ions content causes a continuing growth of the crystalline size, then a little tiny bit decrease is observed for x = 0.20. Many factors could influence the variation of the lattice, and the main reasons are ascribed to the valence state of the dopant ions and the crystalline size. Generally speaking, a lattice contraction will be observed when increasing the crystalline size due to microstrain effects existing in nanosized materials[28]. Combined with the results of Fig. 2(a) and 2(c), we can see that although the crystalline sizes keep growing, the cell parameters still grow with straight line, which implies that the doped ion contents are the primary cause for affecting the cell parameters.

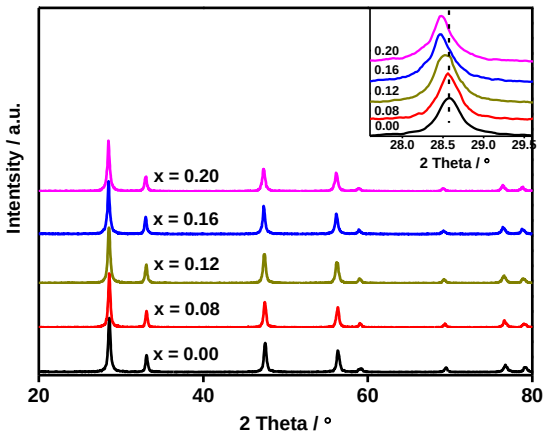

Fig. 1. XRD patterns of the typical Nd^{3+} and Eu^{3+} co-doped CeO_2 samples, inset shows enlarged XRD patterns for the (111) peak

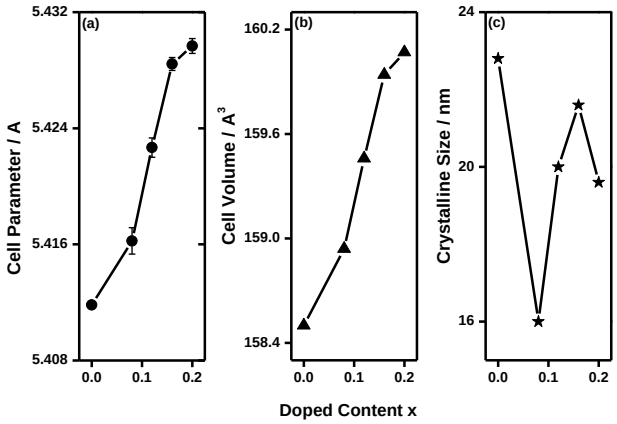

Fig. 2. Doped content dependence of (a) cell parameters, (b) cell volume and (c) crystallite size

3. 2 Raman spectra

Raman measurement is a kind of nondestructive, sensitive, and rapid analysis technique to research on

phonon and the electronic structure of materials. Any changes in lattice spacing or chemical environment will induce the band frequencies to shift. CeO_2 shows a cubic fluorite structure and belongs to O_h^5 space group. The doping of Nd^{3+} and Eu^{3+} ions into the lattice of CeO_2 deforms the structure and can be tested by Raman spectra. Fig. 3 displays the Raman spectra of typical $Ce_{1-x}(Nd_{0.5}Eu_{0.5})_xO_{2-\delta}$ solid solutions. All the solid solutions display one sharp and strong band around 453 cm^{-1} ascribing to Raman-active F_{2g} mode, which is the feature of fluorite structural materials corresponding to the oxygen breathing vibrations around the Ce^{4+} ions[29]. The shift of F_{2g} Raman mode for the doped solid solutions to larger wavenumbers ascribes to the crystalline size effect and the lattice distortion[30]. Moreover, a broad and weak peak located around 570 cm^{-1} ascribing to the characteristic of oxygen vacancies in the lattice of $Ce_{1-x}(Nd_{0.5}Eu_{0.5})_xO_{2-\delta}$ solid solutions is also monitored by Raman technique, and the intensity of this peak is increased by increasing the doped content.

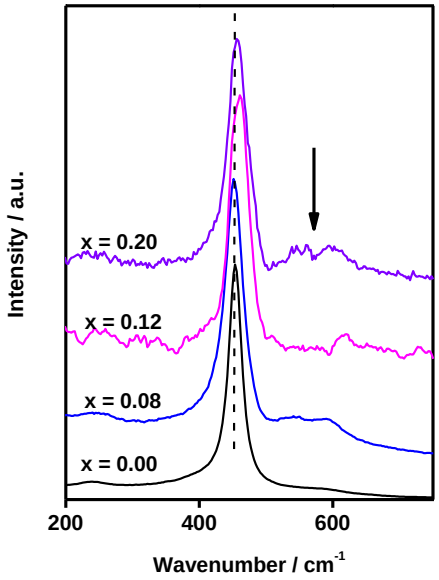

Fig. 3. Raman spectra of $Ce_{1-x}(Nd_{0.5}Eu_{0.5})_xO_{2-\delta}$ solid solutions

3. 3 UV-Vis spectrum analysis

The UV-Vis absorption spectra of the $Ce_{1-x}(Nd_{0.5}Eu_{0.5})_xO_{2-\delta}$ (x = 0.00～0.20) solid solutions are shown in Fig. 4(a). It can be found that the pure CeO_2 has no absorption in the visible region, while the doped samples exhibit extra absorption peaks, and the intensities of the bands become more distinct with increasing the Nd^{3+} and Eu^{3+} concentrations. The weak bands located at 520 and 534 nm correspond to the 4*f*-4*f* transitions from the $^7F_{0,1}$ level to the excited states of Eu^{3+} ions. More specifically, the absorption band at 520 nm due to $^7F_0 \rightarrow {}^5D_1$ transition and the $^7F_1$ state to $^5D_1$ are present at 535 nm[30]. On the other hand, the absorption bands with relatively higher intensity centered at around 590, 685 and 745 nm correspond to the Nd^{3+} ion transitions starting from the $^4I_{9/2}$ ground state to the higher levels $^4G_{5/2} + {}^4G_{7/2}$, $^4F_{9/2}$, $^4F_{7/2} + {}^4S_{3/2}$, respectively[31]. Fig. 4(b) displays the bandgap energies of the typically synthesized samples which are calculated using the Tauc relation as shown in Eq. (1) considering the direct allowed transition[32].

$$\alpha h\nu = A(h\nu - E_g)^{1/2} \quad (1)$$

where α is the absorption coefficient, and A is the constant. It can be seen that the bandgap energies almost decrease linearly from 3.23 eV for x = 0.00 to 2.81 eV for x = 0.20. The reason could be ascribed to the replacement of Ce^{4+} with lower valence states of Eu^{3+} and Nd^{3+}, which will result in the formation of oxygen vacancies and additional energy levels. Besides, the doping causes the lattice distortion which could also affect the bandgap structure. This result is in accordance with that of the Raman analysis which means that Eu^{3+} and Nd^{3+} have doped into the lattice of CeO_2 successfully and affected the lattice structure as well as changing the performance of electron transition.

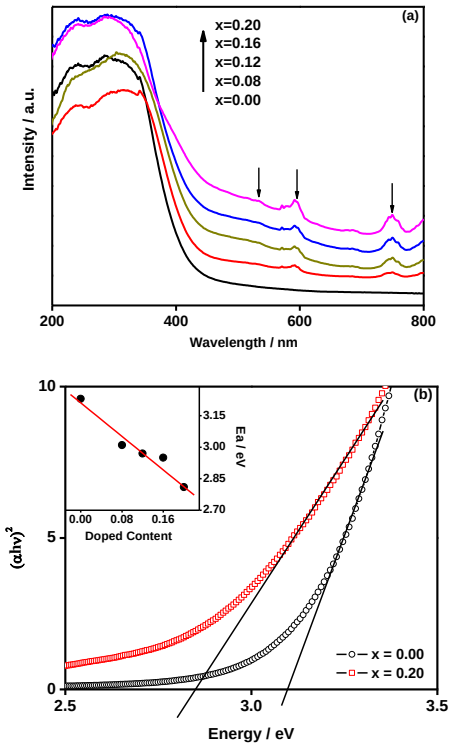

Fig. 4. (a) UV-Vis absorption spectrum of the $Ce_{1-x}(Nd_{0.5}Eu_{0.5})_xO_{2-\delta}$ (x = 0.00～0.20) solid solutions; (b) Band gap energy of the samples

3. 4 Microstructure of the Mg_2Ni-Ni-5% $Ce_{1-x}(Nd_{0.5}Eu_{0.5})_xO_{2-\delta}$ composites

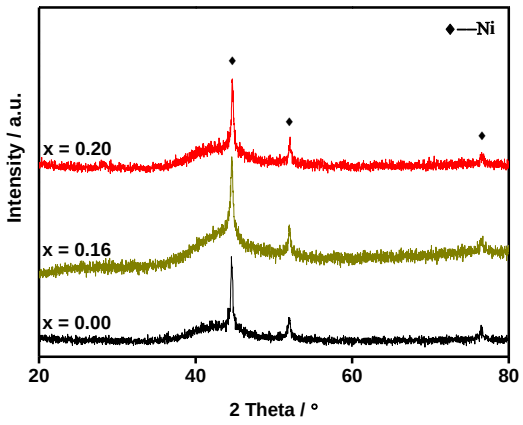

Fig. 5. XRD pattern ball milled Mg_2Ni-Ni-5% $Ce_{1-x}(Nd_{0.5}Eu_{0.5})_xO_{2-\delta}$ composites

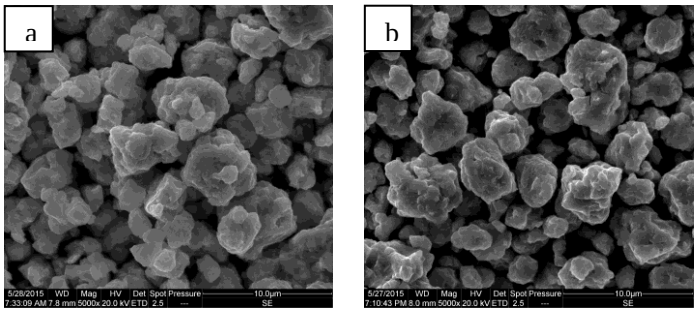

Fig. 6. SEM pictures of the Mg_2Ni–Ni–5% $Ce_{1-x}(Nd_{0.5}Eu_{0.5})_xO_{2-\delta}$ composites, (a) x = 0.16 ; (b) x = 0.20

Fig. 5 displays the XRD patterns of Mg_2Ni–Ni–5% $Ce_{1-x}(Nd_{0.5}Eu_{0.5})_xO_{2-\delta}$ composites after ball milled for 20 h. It can be seen that the Mg_2Ni alloys exhibit amorphous/nanocrystalline phase and the Ni powders to some extent still display as the crystalline phase (PDF#70-0989). However, the phases of $Ce_{1-x}(Nd_{0.5}Eu_{0.5})_xO_{2-\delta}$ can not be observed which could be ascribed to the small amount of catalysts. The morphologies of the ball milled composites shown in Fig. 6 indicate that the particle sizes of samples were uniformity and the radius being about 5 μm. By comparing the XRD and SEM results, it seems that there are no significant distinctions in the morphologies of the composites with various catalysts. Therefore, different electrochemical and kinetic performances of the composites will be discussed followed could be put down to the catalysis effects of the $Ce_{1-x}(Nd_{0.5}Eu_{0.5})_xO_{2-\delta}$ catalysts with diverse doped content.

3. 5 Electrochemical properties of Mg_2Ni–Ni–5% $Ce_{1-x}(Nd_{0.5}Eu_{0.5})_xO_{2-\delta}$ composites

Fig. 7(a) gives the first cycle discharge curves of the ball milled Mg_2Ni–Ni–5% $Ce_{1-x}(Nd_{0.5}Eu_{0.5})_xO_{2-\delta}$ composites. The discharge potential plateau corresponds to the oxidation process of desorbed hydrogen from Mg_2NiH_4. Compared with the catalytic effect between the solid solutions with different doped content, it clearly shows that the widths of discharge potential plateau of the samples with doped catalysts are larger than that with pure CeO_2. Specifically, the discharge capacity fist increases from 722.3 mAh/g for x = 0.00 to 819.7 mAh/g for x = 0.16, and then slightly decreases to 780.1 mAh/g for x = 0.20. This result means that the doped $Ce_{1-x}(Nd_{0.5}Eu_{0.5})_xO_{2-\delta}$ could help to enhance the discharge capacities compared with that of using pure CeO_2 as the catalyst. Meanwhile, it should be noticed that the electrodes with the $Ce_{1-x}(Nd_{0.5}Eu_{0.5})_xO_{2-\delta}$ (x = 0.00, 0.12, 0.16) catalysts are almost similar in middle potential, but the composites electrodes (x = 0.08, 0.20) shift to higher potential and decrease steeper in the process of discharging. The reason of the variation of plateau slop can be ascribed to the various amorphous tendency of the composites with different catalysts[33].

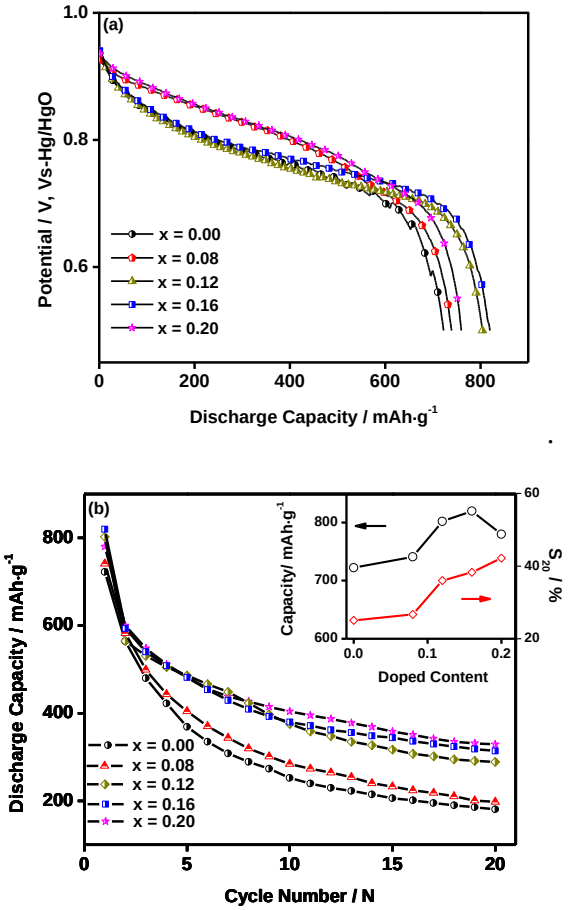

Fig. 7. Electrochemical properties of Mg_2Ni–Ni–5% $Ce_{1-x}(Nd_{0.5}Eu_{0.5})_xO_{2-\delta}$ composites
(a) the first cycle discharge curves; (b) the cycle stability and the capacity retention rate (inset)

The cycle stability of the composites electrodes is one of the most important features which directly affect the working life of the batteries. On the other hand, the activation characteristic and the maximum discharge capacity are also two factors which are closely associated with their practical applications. Fig. 7(b) depicts the cyclic stability curves, and the inset presents the maximum discharge capacity and the capacity retention rate S_{20} of the ball milled composites. It can be seen that all the composites can be activated in the first cycle. The maximum discharge capacities of the composites with doped $Ce_{1-x}(Nd_{0.5}Eu_{0.5})_xO_{2-\delta}$ solid solutions are higher than that with pure CeO_2. Meanwhile, the discharge capacity retention rates S_{20} also increase from 25.0% (x = 0.00) to 42.2% (x = 0.20). With regard to Mg_2Ni based composites, the main reason for the degradation of discharge capacity closely relays on the corrosion of active alloy in alkaline electrolyte. The optimization of the cycle stability indicated the doped solid solutions are probably improving the corrosion resistance of Mg_2Ni alloys.

3. 6 Electrochemical kinetic properties

Fig. 8(a) gives the EIS Nyquist plots of Mg_2Ni–Ni–5% $Ce_{1-x}(Nd_{0.5}Eu_{0.5})_xO_{2-\delta}$ composites electrodes in 50% DOD. It can be seen that every curve consists of two semicircles and a linear Warburg impendence. The

larger semicircle in middle frequency region corresponds to the charge transfer process on the electrode surface. And it can be considered as the rate control step at the interface between the alloy and the electrolyte. Generally speaking, the rate of charge transfer is depending on the crystallographic and electronic structure[35]. The different constitutes on the surface of alloy will affect the distribution of valence electron, which substantially influences the hydrogen dissociation reaction[36]. The composites with doped $Ce_{1-x}(Nd_{0.5}Eu_{0.5})_xO_{2-\delta}$ (x > 0.00) exhibit a visible shrink in the radius of the larger semicircle, demonstrating that the doped catalyst acts a positive role on the rate of charge transfer. Concretely, the order is as follows: x = 0.20 > 0.16 > 0.12 > 0.08 > 0.00, which means that the catalytic activities of the doped solid solutions are consistent with the doped content.

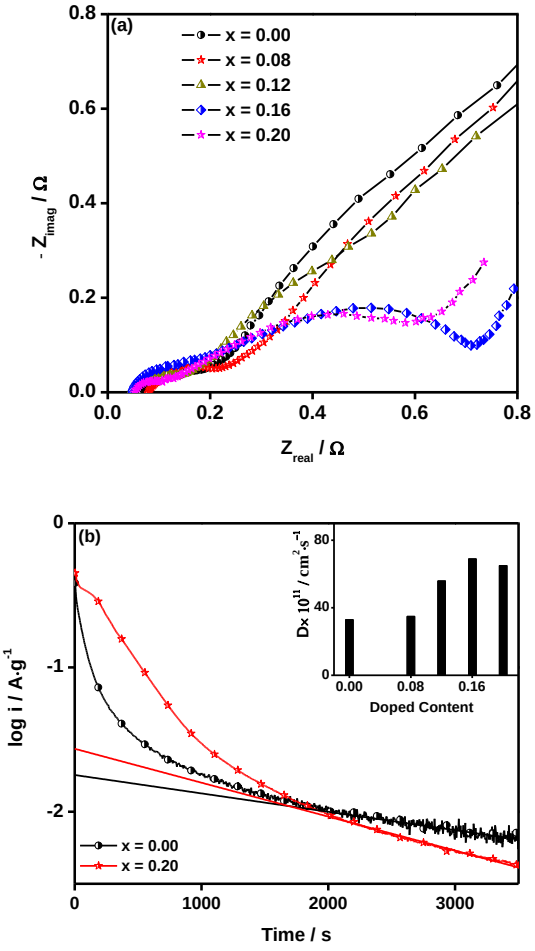

Fig. 8. Kinetic properties of Mg_2Ni–Ni–5% $Ce_{1-x}(Nd_{0.5}Eu_{0.5})_xO_{2-\delta}$ composites electrodes (a) EIS Nyquist plots in 50% DOD; (b) Semilogarithmic curves of anodic current *vs.* time responses in 100% DOD, and the inset shows the diffusion coefficient *D* with different doped catalysts

In order to assess the hydrogen diffusivity, the typical semilogarithmic curves of anodic current log(i) *vs.* discharge time (t) of the electrodes with 100% DOD are depicted in Fig. 8(b). From the slope of log(i) with t, we can obtain the hydrogen diffusion coefficient D to be 10 μm by assuming the average radius of

composites[37]. As seen in the inset of Fig. 8(b), the *D* increases firstly and then decreases a bit with increasing the doped content, which means that the catalysts with different contents influence the *D* obviously.

3. 7 Explanation of catalysis mechanism

As is discussed before, the electrochemical and kinetic properties of the Mg_2Ni–Ni–5% $Ce_{1-x}(Nd_{0.5}Eu_{0.5})_xO_{2-\delta}$ composites are improved remarkably, which means the Eu^{3+} and Nd^{3+} co-doped catalysts play a positive role in promoting the hydrogen storage properties of Mg_2Ni alloy. The catalysis mechanism can be analyzed from the point of the microstructure and the spectra characteristics. As is analyzed from the XRD, Raman and UV spectra, the enlargement of cell parameters, the distortion of lattice structure, the increasing content of oxygen vacancies and the decreased bandgap energies with increasing the doped content of the catalysts can be taken as the reasons for improving the hydrogen storage properties of Mg_2Ni alloys.

As regards the cell parameters, Chafi et al.[22] proposed that H can be easily adsorbed along the (110) surface of CeO_2 without energy consumption. Thus, the increased cell parameters mean H atoms have larger space to penetrate and allow more H atoms to enter. In other words, the H atoms first choose to enter into the lattice of CeO_2-based catalysts instead of passing through the $Mg(OH)_2$ or MgO layers, which is the main reason of slow sorption/desorption kinetics of Mg-based alloys. When the H atoms are absorbed, the Mg–H bond of the formed Mg_2NiH_4 is still affected by the catalysts. The electron orbitals have close interaction between the catalysts and the Mg_2NiH_4, and the electronic exchange reactions result in the triggered Mg–H bond, which accelerates the dissociation of Mg_2NiH_4. The narrowed band gap energies of the catalysts could enhance the electronic exchange interaction and therefore facilitate the decomposed of Mg–H bond[21]. With respect to the oxygen vacancy, the catalytic activity mainly depends on the content of them. The oxygen vacancies and small polarons of the vacant structure of CeO_2 can help improve the hydrogen desorption kinetics. Borgschulte et al.[38] demonstrated that the desorption properties of MgH_2 can be considered as a function of the oxygen vacancy formation. Oelerich et al.[4] also investigated that the oxides with different valences exhibited superior catalytic effect. Thus, in our experiment, we doped two ions with different valence and size into the lattice of CeO_2, which could not only increase the number of oxygen vacancies but also make the metal atoms display various electronic states. Meanwhile, the $Ce_{1-x}(Nd_{0.5}Eu_{0.5})_xO_{2-\delta}$ solid solutions keep with the fluorite structure single phase, allowing the rapider diffusion of oxygen atoms to locate at the same crystallographic plane, which is also an important benchmark of the catalytic activity. On the other hand, it is worth noting that although the degree of the lattice distortion, the band gap energy and the oxygen vacancies content change almost linearly, the variation of some corresponding hydrogen storage properties of the composites is not following the same tendency. Specifically, the maximum discharge capacity and the value of diffusion coefficient *D* of the composites with $x = 0.20$ are lowered than that of $x = 0.16$. During the ball milling process, the nanosized catalysts will attach on the surface of Mg_2Ni alloys, and different size of the catalyst will affect their distribution, which influences the surface activity of the alloy further. As is indicated

in the XRD pattern, the size of catalysts first increases and then decreases with x = 0.20; the variation of the maximum discharge capacity and D value follows almost the same trend. This tendency means that various crystalline sizes of the catalysts may also influence their catalysis effects, and the specific reason needs to be researched further.

4 CONCLUSION

The nanosized Eu^{3+} and Nd^{3+} co-doped $Ce_{1-x}(Nd_{0.5}Eu_{0.5})_xO_{2-\delta}$ solid solutions are synthesized via hydrothermal method. Their microstructures and spectral characteristics are analyzed systematically. After that, ball milled Mg_2Ni–Ni–5% $Ce_{1-x}(Nd_{0.5}Eu_{0.5})_xO_{2-\delta}$ composites are obtained by ball milling method, and the electrochemical and kinetic properties of the composites are investigated. The $Ce_{1-x}(Nd_{0.5}Eu_{0.5})_xO_{2-\delta}$ solid solutions show fluorite cubic CeO_2 phase without any additional phases in the doped range $x \leqslant 0.20$. With increasing doped content, the cell parameters and cell volumes are enlarged, the oxygen vacancy concentrations are increased, and the bandgap energies are decreased. The doped solid solutions could improve the electrochemical and kinetic properties of Mg_2Ni alloy. The maximum discharge capacity was increased from 722 mAh/g for x = 0.00 to 819.7 mAh/g for x = 0.16, and the cycle stability S_{20} increased from 25.0% (x = 0.00) to 42.2% (x = 0.20). The kinetic measurement proved that the catalytic activity of composites surfaces and the hydrogen diffusion rate were improved for the composites with doped catalysts, especially for the composites with x = 0.16 and x = 0.20. The catalytic mechanism is analyzed from the microstructure and the spectrum feature of the catalysts. It is found that the doped solid solutions catalysts with larger cell parameters, the distorted lattice structures, the increasing content of oxygen vacancies and the decreased bandgap energies can be taken as the optimized factors for improving the electrochemical hydrogen storage properties of Mg_2Ni alloys.

REFERENCES

(1) Bardhan, R.; Ruminski, A. M.; Band, A.; Urban, J. J. Magnesium nanocrystalpolymer composites: a new platform for designer hydrogen storage materials. *Energy Environ. Sci*. **2011**, 4, 4882–4895.

(2) Barkhordarian, G.; Klassen, T.; Bormann, R. Catalytic mechanism of transition metal compounds on Mg hydrogen sorption reaction. *J. Phys. Chem. B* **2006**, 110, 11020–11024.

(3) Chu, H. L.; Qiu, S. J.; Tian, Q. F.; Sun, L. X.; Zhang, Y.; Xu, F.; Liu, Y. Y.; Qi, Y. N.; Fan, M. Q. Effect of ball milling time on the electrochemical properties of La-Mg-Ni-based hydrogen storage composite alloys. *Int. J. Hydrogen Energy* **2007**, 32, 4925–4932.

(4) Oelerich, W.; Klassen, T.; Bormann, R. Metal oxides as catalysts for improved hydrogen sorption in nanocrystalline Mg-based materials. *J. Alloys Compd*. **2001**, 315, 237–242.

(5) Oelerich, W.; Klassen, T.; Bormann, R. Comparison of the catalytic effects of V, V_2O_5, VN, and VC on the hydrogen sorption of nanocrystalline Mg. *J. Alloys Compd*. **2001**, 322, L5–L9.

(6) Hanada, N.; Ichikawa, T.; Isobe, S.; Nakagawa, T.; Tokoyoda, K.; Honma, T.; Fujii, H.; Kojima, Y. X-ray absorption spectroscopic study on valence state and local atomic structure of transition metal oxides doped in MgH_2. *J. Phys. Chem. C* **2009**, 113, 13450–13455.

(7) Borgschulte, A.; Bosenberg, U.; Barkhordarian, G.; Dornheim, M.; Bormann, R. Enhanced hydrogen sorption kinetics of magnesium by destabilized

MgH_2. *Catal. Today* **2007**, 120, 262−269.

(8) Heck, R. M.; Farrauto, R. J. Automobil exhaust catalysts. *Appl. Catal., A* **2001**, 221, 443−457.

(9) Chen, H. Y.; Chang, H. L. Development of low temperature three-way catalysts for future fuel efficient vehicles. *Johnson Matthey Technol. Rev.* **2015**, 59, 64−67.

(10) Ratnasamy, C.; Wagner, J. P. Water gas shift catalysis. *Catal. Rev*. **2009**, 51, 325−440.

(11) Trovarelli, A. Catalytic properties of ceria and CeO_2-containing material. *Catal. Rev. Sci. Eng*. **1996**, 38, 439−520.

(12) Liu, S.; Wu, X. D.; Weng, D.; Ran, R. Ceria-based catalysts for soot oxidation: a review. *J. Rare Earths* **2015**, 33, 567−590.

(13) Malecka, M. A.; Kepinski, L.; Mista, W. Structure evolution of nanocrystalline CeO_2 and $CeLnO_x$ mixed oxides (Ln = Pr. Tb, Lu) in O_2 and H_2 atmosphere and their catalytic in soot comnistion. *Appl. Catal., B* **2007**, 74, 290−298.

(14) Krishna, K.; Bueno-lopez, A.; Makkee, M.; Moulijin, J. Potential rare earth modified CeO_2 catalysts for soot oxidation: I. Characterization and catalytic activity with O_2. *Appl. Catal., B* **2007**, 75, 189−200.

(15) Panagiotou, G. D.; Petsi, T.; Bourikas, K.; Kalampounias, A. G.; Boghosian, S.; Kordulis, C.; Lycourghiotis, A. Interfacial impregnation chemistry in the synthesis of molybdenum catalysts supported on titania. *J. Phys. Chem. C* **2010**, 114, 11868−11879.

(16) Peng, C.; Wang, Y.; Jiang, K.; Bin, B. Q.; Liang, H. W.; Feng, J.; Meng, J. Study on the structure change and oxygen vacation shift for $Ce_{1-x}Sm_xO_{2-y}$ solid solution. *J. Alloys Compd*. **2003**, 349, 273−278.

(17) Bai, W.; Choy, K. L.; Stelzer, N. H. J.; Schoonman, J. Thermophoresis-assisted vapour phase synthesis of CeO_2 and $Ce_xY_{1-x}O_{2-\delta}$ nanoparticles. *Solid State Ion* **1999**, 116, 225−228.

(18) Sin, A.; Dubitsky, Y.; Zaopo, A.; Aric òA. S.; Gullo, L.; La, Rosa, D.; Siracusano, S.; Antonucci, V.; Oliva, C.; Ballabio, O. Preparation and sintering of $Ce_{1-x}Gd_xO_{2-x/2}$ nanopowders and their electrochemical and EPR characterization. *Solid State Ion* **2004**, 175, 361−366.

(19) Song, M. Y.; Bobet, J. L.; Darriet, B. Improvement in hydrogen sorption properties of Mg by reactive mechanical grinding with Cr_2O_3, Al_2O_3 and CeO_2. *J. Alloys Compd*. **2002**, 340, 256−262.

(20) Janot, R.; Darok, X.; Rougier, A.; Aymard, L.; Nazrinn, G. A.; Tarascon, J. M. Hydrogen sorption properties for surface treated MgH_2 and Mg_2Ni alloys. *J. Alloys Comps*. **2005**, 404−406, 293−296.

(21) Gulicovski, J.; Raskovic-Lovre, Z.; Kurko, S.; Vujasin, R.; Jovanovic, Z.; Matovic, L.; Noovakovic, J. G. Influence of vacant CeO_2 nanostructured ceramics on MgH_2 hydrogen desorption properties. *Ceram. Int*. **2012**, 38, 1181−1186.

(22) Chafi, Z.; Keghouche, N.; Minot, C. Density function theoretical study of interaction of hydrogen with ceria. *Phys. Procedia*. **2009**, 2, 673−676.

(23) Zhang, G. F.; Xv, J. Y.; Hou, Z. H.; Wang, Q. C. Research on micro-structure and catalysis properties of nanosized $Ce_{1-x}(Fe_{0.5}Eu_{0.5})_xO_{2-\delta}$ solid solutions. *J. Rare Earth* **2017**, 35, 63−70.

(24) Xiong, Y. P.; Yamaji, K.; Horita, T.; Sakai, N.; Yokokawa, H. Hole and electron conductivities of 20 mol% - $REO_{1.5}$ doped CeO_2 (RE = Yb, Y, Gd, Sm, Nd, La). *J. Electrochem. Soc*. **2004**, 151, A407−A412.

(25) Palmqvist, A. E. C.; Johansson, E. M.; J ä ås, M.; Muhammed, S. G. Total oxidation of methane over doped nanophase cerium oxides. *Catal. Let*. **1998**, 56, 69−75.

(26) Hern ández, W. Y.; Centeno, M. A.; Romero-Sarria, F.; Odriozola, J. A. Synthesis and characterization of $Ce_{1-x}Eu_xO_{2-x/2}$ mixed oxides and their catalytic activities for CO oxidation. *J. Phys. Chem. C* **2009**, 113, 5629−5635.

(27) Li, R. X.; Yabe, S.; Yamashita, M.; Momose, S.; Yoshida, S.; Yin, S.; Sato, T. Synthesis and UV-shielding properties of ZnO- and CaO-doped CeO_2 via soft solution chemical process. *Solid State Ion* **2002**, 151, 235−241.

(28) Tsunekawa, S.; Sivamohan, R.; Ito, S.; Kasuya, A.; Fukuda, T. Structural study on monosize CeO_{2-x} nano-particles. *Nanostruct. Mater*. **1999**, 11, 141−147.

(29) Keramidas, V. G.; White, W. B. Raman spectra of oxides with the fluorite structure. *J. Chem. Phys*. **1973**, 59, 1561−1562.

(30) Walas, M.; Lewandowski, T.; Synak, A.; Łapiński, M.; Sadowski, W.; Kościelska, B. Eu^{3+} doped tellurite glass ceramics containing SrF_2 nanocrystals: preparation, structure and luminescence properties. *J. Alloy. Compd*. **2017**, 696, 619−626.

(31) Chen, R.; Tian, Y.; Li, B. P.; Huang, F. F.; Wang, C. Z.; Jing, X. F.; Zhang, J. J.; Xu, S. Q. Efficient 2 μm emission in Nd^{3+}/Ho^{3+} co-doped silicate-germanate glass pumped by common 808 nm LD. *Opt. Laser Technol*. **2017**, 89, 108−113.

(32) Daghrir, R.; Drougui, P.; Robert, D.; Modified TiO_2 for environmental photocatalytic applications: a review. *Ind. Eng. Chem. Res*. **2013**, 52, 3581−3599.

(33) Li, R.; Wan, J.; Wang, F.; Ding, C.; Yu, R. Effect of non-stoichiometry on microstructure and electrochemical performance of $La_{0.8}Gd_xMg_{0.2}Ni_{3.15}Co_{0.25}Al_{0.1}$ (x = 0～0.4) hydrogen storage alloys. *J. Power Sources* **2016**, 301, 229−236.

(34) Iwakura, C.; Matsuoka, M.; Asai, K.; Kohno, T. Surface modification of metal hydride negative electrodes and their charge/discharge performance. *J. Power Source* **1992**, 38, 335−343.

(35) Kleperis, J.; Wojcik, G.; Czerwinski, A.; Skiwronski, J.; Kopczyk, M.; Beltowska-brzezinska, M. Electrochemical behavior of metal hydrides. *J. Solid State Electrochem.* **2001**, 5, 229−249.

(36) Nobuhara, K.; Kasai, H.; Dino, W. A.; Nakanishi, H. H_2 dissociative adsorption on Mg, Ti, Ni, Pd and La surface. *Surf. Sci*. **2004**, 566–568, 703–707.

(37) Zheng, G.; Popov, B. N.; White, R. E. Electrochemical determination of the diffusion coefficient of hydrogen through an $LaNi_{4.25}Al_{0.75}$ electrode in alkaline aqueous solution. *J. ElectrocheM. Soc*. **1995**, 142, 2695–2698.

(38) Borgschulte, A.; Bielmann, M.; Zuttel, A.; Barkhordarian, G.; Dornheim, M.; Bormann, R. Hydrogen dissociation on oxide covered MgH_2 by catalytically active vacancies. *Appl. Surf. Sci.* **2008**, 254, 2377–2384.

Role of Microstructure and Spectrum Features on the Catalysis Effect of $Ce_{1-x}(Nd_{0.5}Eu_{0.5})_xO_{2-\delta}$ Solid Solutions

ZHANG Guo-Fang(张国芳) HOU Zhong-Hui(侯忠辉) ZHAI Ting-Ting(翟亭亭)

XV Jian-Yi(许剑轶) ZHANG Yang-Huan(张羊换)

Nanosized $Ce_{1-x}(Nd_{0.5}Eu_{0.5})_xO_{2-\delta}$ solid solutions (x = 0.00～0.20) were synthesized by means of hydrothermal method. Then the solid solutions were ball milled with Mg_2Ni and Ni powders for 20 h to get the Mg_2Ni–Ni–5 mol% $Ce_{1-x}(Nd_{0.5}Eu_{0.5})_xO_{2-\delta}$ composites. The maximum discharge capacity of the composites was increased from 722.3 mAh/g for x = 0.00 to 819.7 mAh/g for x = 0.16, and the cycle stability S_{20} increased from 25.0% (x = 0.00) to 42.2% (x = 0.20). The kinetic measurement proved that the catalytic activity of composites surfaces and the hydrogen diffusion rate were improved for the composites with doped catalysts, especially for the composites with x = 0.16 and x = 0.20.